



Growth kinetics of hexagonal sub-micrometric β -tricalcium phosphate particles in ethylene glycol [☆]



Laetitia Galea ^{a,b}, Marc Bohner ^{a,*}, Juerg Thuerling ^{a,c}, Nicola Doebelin ^a, Terry A. Ring ^d, Christos G. Aneziris ^b, Thomas Graule ^{b,e}

^a RMS Foundation, Bischmattstrasse 12, CH-2544 Bettlach, Switzerland

^b Technical University Bergakademie Freiberg, Institute for Ceramic, Glass- and Construction Materials, Agricolastraße 17, 09596 Freiberg, Germany

^c ETH Zürich, Department of Materials, Laboratory of Multifunctional Materials, Wolfgang-Pauli-Strasse 10, 8093 Zürich, Switzerland

^d University of Utah, Chemical Engineering, 50 South Central Campus Drive, Salt Lake City, UT 84112-9203, USA

^e EMPA, Swiss Federal Laboratories for Materials Science and Technology, Laboratory for High Performance Ceramics, Ueberlandstrasse 129, 8600 Dübendorf, Switzerland

ARTICLE INFO

Article history:

Available online 13 March 2014

Keywords:

Calcium phosphate
Bone substitute
Growth kinetics
Reaction-controlled
Ethylene glycol

ABSTRACT

Recently, uniform, non-agglomerated, hexagonal β -tricalcium phosphate (β -TCP) platelets (diameter \approx 400–1700 nm, $h \approx$ 100–200 nm) were obtained at fairly moderate temperatures (90–170 °C) by precipitation in ethylene glycol. Unfortunately, the platelet aspect ratios (diameter/thickness) obtained in the latter study were too small to optimize the strength of polymer- β -TCP composites. Therefore, the aim of the present study was to investigate β -TCP platelet crystallization kinetics, and based on this, to find ways to better control the β -TCP aspect ratio. For that purpose, precipitations were performed at different temperatures (90–170 °C) and precursor concentrations (4, 16 and 32 mM). Solution aliquots were retrieved at regular intervals (10 s–24 h), and the size of the particles was measured on scanning electron microscopy images, hence allowing the determination of the particle growth rates. The β -TCP platelets were observed to nucleate and grow very rapidly. For example, the first crystals were observed after 30 s at 150 °C, and crystallization was complete within 2 min. The crystal growth curves could be well-fitted with both diffusion- and reaction-controlled equations, but the high activation energies (\sim 100 kJ mol⁻¹) pointed towards a reaction-controlled mechanism. The results revealed that the best way to increase the diameter and aspect ratio of the platelets was to increase the precursor concentration. Aspect ratios as high as 14 were obtained, but the synthesis of such particles was always associated with the presence of large fractions of monetite impurities.

© 2014 Acta Materialia Inc. Published by Elsevier Ltd. All rights reserved.

1. Introduction

When bone defects exceed a critical size, bone grafting has to be applied in addition to osteosynthesis to achieve bone healing. The most common source of bone graft is from the patient's iliac crest, but availability is limited and the harvesting procedure causes additional costs, longer operation times and pain at the donor site [1,2]. Allografts might be used to replace or complement the autograft, but this approach raises ethical concerns and may lead to disease transmission [3]. Synthetic bone graft substitute materials are increasingly used in combination with or even in the replacement of grafts [4]. Calcium-based ceramics, and in particular the calcium

phosphates (CaP), are among the most widely used synthetic materials. These materials have attracted great interest because of their chemical similarity to the mineral component of bone [5,6], and their good biological properties such as biocompatibility, osteoconduction and for some of them an active degradation pathway [6,7]. However, their inherent brittleness excludes their use in load-bearing locations and requires supplementary fixation with osteosynthesis fixation devices such as metallic plates and screws [8,9].

One approach to obtain strong and tough bone graft substitutes based on calcium phosphate ceramics would be to mimic the composition and structure of certain natural materials such as bone and nacre [10–12]. These materials can be seen as a ductile organic matrix reinforced with sub-micron ceramic particles or as inorganic particles held together by an organic “glue”. Their architecture is very important and very well controlled [13–15]. For example, the ceramic particles must be below a critical thickness

[☆] Part of the Biomineralization Special Issue, organized by Professor Hermann Ehrlich.

* Corresponding author. Tel.: +41 32 6441413.

E-mail address: marc.bohner@rms-foundation.ch (M. Bohner).

and present a large aspect ratio (particle length/thickness) [16]. Indeed, limiting the size of the ceramics is the most efficient way to increase their strength (Griffith's law) [17]. In the case of β -tricalcium phosphate (β -TCP; β -Ca₃(PO₄)₂), its thickness should not exceed 350 nm. Also, a high aspect ratio provides a good load transfer between organic matrix and ceramic particles but a certain critical aspect ratio should not be exceeded to avoid brittle failure of the composite. In fact, Gao showed that this critical aspect ratio depends on the mechanical properties of the ceramic and the shear strength of the interface between organic material and ceramic [18]. For abalone nacre, the critical aspect ratio of the calcium carbonate crystals is close to 9 and the observed value is 8 [12,19]. For stronger ceramics like alumina platelets in biopolymers, the critical aspect ratio is close to 50 [12]. Calcium phosphates like β -TCP platelets in biopolymers would have a critical aspect ratio between 20 and 25 (theoretical calculations are provided in the [Supplementary data](#)).

With the aim of producing CaP in the form of platelets with controllable thickness and aspect ratio, a precipitation method proposed by Tao et al. [20] was slightly modified [21]. In the latter study, results revealed that two types of particles could be obtained. The first type was highly uniform, non-agglomerated, sub-micrometric β -TCP. Unfortunately, the aspect ratio was relatively limited (typically below 10), and impurities (in the form of secondary phases) were found as soon as the aspect ratio reached values higher than ~ 5 . The second phase was monetite particles (CaHPO₄) with high aspect ratio (typically ~ 20). However, the particles were less monodisperse, less uniform and more agglomerated than the β -TCP particles. Since the latter factors are of paramount importance for the synthesis of nacre-like materials, it appears more promising to focus on β -TCP synthesis as a first step towards the production of nacre-like materials. However, this implies a better control of β -TCP growth mechanisms. Therefore, the aim of the present study was to gain a better understanding of the growth mechanisms of β -TCP platelets with the hope that their aspect ratio would be more easily controlled. Specifically, the time evolution of β -TCP platelets was analyzed as a function of precursor concentration and temperature, and the reaction rates were calculated and compared to various growth kinetic models.

2. Theory

In 2011, Kwon and Hyeon [22] discussed the growth kinetics of uniform nanocrystals. These authors postulated that the particle growth rate could be expressed by Eqs. (1) and (2) for reaction-controlled and diffusion-controlled reactions, respectively:

$$\frac{dr}{dt} = V_m \cdot k \cdot ([M]_b - [M]_r) \quad (\text{reaction-controlled}) \quad (1)$$

$$\frac{dr}{dt} = \frac{D \cdot V_m}{r} \cdot ([M]_b - [M]_r) \quad (\text{diffusion controlled}) \quad (2)$$

where r is the particle radius, t the reaction time, D the diffusion coefficient, V_m the molecular volume (molecular mass, MM , divided by the density, ρ ; $MM = 310 \text{ g mol}^{-1}$ and $\rho = 3.07 \text{ g cm}^{-3}$ for β -TCP), $[M]_b$ the concentration in the bulk, $[M]_r$ the solubility of the spherical particle of radius r and k the reaction rate constant. Considering the low solubility of β -TCP in ethylene glycol (β -TCP readily precipitates at a concentration of 1.6 mM [21] whereas most experiments are performed at 16 mM), it can be assumed that $[M]_r = 0$. If all the particles are formed simultaneously, $[M]_b$ is equal to the difference between the initial concentration, $[M]_0$, and the concentration that has been consumed by the particles already formed:

$$[M]_b = [M]_0 - n \cdot \frac{4}{3} \cdot \pi \cdot r^3 \cdot \frac{\rho}{V} \quad (3)$$

with n the number of particles and V the total volume. Combining Eqs. (1)–(3) leads to Reactions (4) and (5):

$$\frac{dr}{dt} = V_m \cdot k \cdot \left([M]_0 - n \cdot \frac{4}{3} \cdot \pi \cdot r^3 \cdot \frac{\rho}{V} \right) \quad (\text{reaction-controlled}) \quad (4)$$

$$\frac{dr}{dt} = \frac{D \cdot V_m}{r} \cdot \left([M]_0 - n \cdot \frac{4}{3} \cdot \pi \cdot r^3 \cdot \frac{\rho}{V} \right) \quad (\text{diffusion-controlled}) \quad (5)$$

At infinite time, i.e. when all precursors are consumed, $[M]_b = 0$, and the particles reach a maximum size, r_∞ , Eqs. (4) and (5) can be written:

$$\frac{dr}{dt} = V_m \cdot k \cdot [M]_0 \cdot \left(1 - \left(\frac{r}{r_\infty} \right)^3 \right) \quad (6)$$

$$r \cdot \frac{dr}{dt} = V_m \cdot D \cdot [M]_0 \cdot \left(1 - \left(\frac{r}{r_\infty} \right)^3 \right) \quad (7)$$

The particles obtained with the present synthesis method are hexagonal prisms, with an inner diameter d_{hex} and a thickness h_{hex} . Therefore, the radius of a sphere of equivalent volume was calculated and used in Eqs. (6) and (7).

$$r = \sqrt[3]{\frac{3}{4} \cdot \left(\frac{d_{hex}}{2} \right)^2 \cdot h_{hex}} \quad (8)$$

In Eqs. (6) and (7), the value of r_∞ can be estimated by calculating the mean size of the particles present at the end of the reaction. As a result, it is possible to calculate the number of particles using Eq. (9):

$$n = [M]_0 \cdot \frac{3}{4\pi} \cdot \frac{V}{\rho \cdot r_\infty^3} \quad (9)$$

The other two unknowns in Eqs. (6) and (7), namely k and D , can be retrieved from a numerical fit of the experimental data. Then, the activation energy, E_a , can be directly calculated from the slope of $\ln(k) = f(1/T)$ or $\ln(D) = f(1/T)$ curves using the Arrhenius' law (Eq. (10)):

$$k = k_0 \cdot \exp\left(\frac{-E_a}{RT}\right) \text{ or } D = D_0 \cdot \exp\left(\frac{-E_a}{RT}\right) \quad (10)$$

where R is the ideal gas constant ($8.314 \text{ J K}^{-1} \text{ mol}^{-1}$) and k_0 and D_0 are constants.

3. Materials and methods

3.1. Materials and sample preparation

CaP platelets were produced using the precipitation method described in Ref. [21]. The phosphate solution was prepared by placing 140 ml of ethylene glycol (C₂H₆O₂, Reag. Ph. Eur., art. no. 85512.360, VWR, Nyon, Switzerland) in a 600 ml glass beaker and heated up to 90–110 °C. Then, 9.52 ml of a 0.0825/0.33/0.66 M Na₂HPO₄ (Na₂HPO₄·2H₂O, purum p.a., art. no. 71645, Fluka, Buchs, Switzerland) solution and 0.21/0.84/1.68 ml of a 1.3 M NaOH (NaOH, puriss. p.a., art. no. 71690, Fluka, Buchs, Switzerland) were added. To prepare the calcium solution, 350 ml of ethylene glycol was mixed with 0.175/0.700/1.4 g CaCl₂·2H₂O (CaCl₂·2H₂O, Reag. Ph. Eur., art. no. 1.02382, MERCK, Darmstadt, Germany) in a 1 l triple-neck round bottom flask connected with a coil condenser and isolated with aluminum foil. This solution was heated to 90–180 °C under intense stirring. The temperatures of both solutions were chosen such as to match the target temperatures upon mixing (ex: 350 ml at 170 °C mixed with 140 ml at 100 °C to reach 150 °C). Thus it can be assumed that the achievement of a

homogeneous temperature lasted as long as it takes to reach a homogeneous mixture. The phosphate solution was poured into the calcium solution within 5 s. In the end, each experiment consisted of a 500 ml solution containing phosphate and calcium ions in 2:3 M ratio with a total $[\text{Ca}^{2+}] + [\text{PO}_4^{3-}]$ ions concentration ranging from 4 mM to 32 mM. The effect of temperature was studied at a concentration of 16 mM by varying the temperature from 90 to 170 °C in 20 °C steps. In some cases, the target temperature could not be reached, so some experiments were also conducted at additional intermediary temperatures. With 4 and 32 mM, reactions were only conducted at 110, 130 and 150 °C. During the experiment, 10 ml aliquots were retrieved at regular intervals (the sampling times were adapted according to the reaction temperature) and placed in a 50 ml PP tube (art. no. 525-0402, VWR, Nyon, Switzerland). These samples were rapidly cooled down by placing the tubes in an ice bath and then centrifuged at 4000 rpm for 30 min to sediment and extract the solid phase. The precipitated crystals were then dispersed and centrifuged in ethanol ($\text{C}_2\text{H}_6\text{O}$, absolute 99.8%, art. no. G003, Grogg, Switzerland), in demineralized water and in ethanol again. After the third washing step, the precipitate was dispersed in 3 ml of ethanol. A drop of this solution was spread over a scanning electron microscopy (SEM) aluminium sample holder and dried in air. SEM observations were performed and the size and aspect ratio of the particles were measured by image analysis of the SEM images (see below).

At the end of the experiment, the remaining suspension was also rinsed by centrifugation as described above and a part of it was used for X-ray diffraction (XRD) measurements (see below). The rest of the suspension was dried at 30 °C under vacuum for 24 h and stored.

Each experiment was repeated at least twice.

3.2. Characterization methods

The particle appearance and size were analyzed by SEM. For this, the samples were coated with a 10 nm thick platinum layer (60 s, 40 mV) and observed with a EVO MA25 microscope (Zeiss, Germany) using a voltage of 20 kV and a working distance of 7–8 mm. The particle size was assessed by image analysis (Image Access 11 Premium, Imagic Bildverarbeitung AG, Glattbrugg, Switzerland) of SEM images at 10,000 \times magnification. Images were taken in regions where some particles were lying flat but also standing on their edge to allow diameter and thickness measurements. A minimum of 15 crystals was used to measure the diameter and a minimum of six crystals to measure the thickness. Only in the case of samples taken at an early reaction stage did the number of measurements have to be reduced because only a few platelets were apparent in the amorphous phase. The diameters of the hexagon prisms, octahedrons and spherical particles were defined as the diameter of the inscribed circle. The size dispersion is calculated as the standard deviation of the particle measurement divided by the average size from image analysis.

The crystalline composition was analyzed by XRD measurements. For this, a concentrated ethanol suspension was dried on a glass plate, scratched off and spread on a silicon single crystal sample holder to minimize preferred orientation. XRD data were collected in reflective geometry on an X'Pert diffractometer (X'Pert Pro MPD, Panalytical, Almelo, The Netherlands). Ni-filtered Cu K_α radiation and a step size of 0.016° were used to measure from 4.01° to 59.99° 2 θ . Due to the limited amount of sample material available, sample transparency, texture and variable irradiated volume limited the quality of the diffraction patterns. Therefore only semi-quantitative phase analyses could be done by Rietveld refinement using the FullProf.2k software (version 5.00) [23] and a previously determined instrument resolution function. Crystalline

models for β -TCP, monetite (DCP) and chloroapatite (Cl-HA) were taken from Schroeder et al. [24], Dickens et al. [25] and Hughes et al. [26].

4. Results

4.1. Visual observations during manipulations

After centrifugation, nothing was observed in the first aliquots retrieved at low concentration and temperature. However, a transparent gel was seen to sediment after a while, particularly at high concentrations. At longer reaction times, this gel was progressively replaced by a white sediment forming at the bottom of the vials. The ratio between the white sediment and the transparent gel increased with time. Moreover, the amount of white sediment appeared to be proportional to the reagent concentration. The typical yield of CaP powder after drying was 0.3–0.4 g l⁻¹.

4.2. SEM observations

At the beginning of the reactions, the first solid identified by SEM was of undefined shape (Fig. 1a). No faceted particles (herein-after called crystals) were detected. The first crystals appeared after a given time which increased with decreasing temperature (Fig. 1b). For example, a few crystals were observed after 30 min of reaction at 90 °C (Fig. S.1), whereas first crystals were already present after 30 s of reaction at 150 °C (Fig. 1b). The crystal size increased with the reaction time, while the amount of solid with undefined shape decreased (Fig. 1). At 90 °C, mostly large parallelepipedic crystals were observed. Nevertheless, some hexagonal platelets were also present (Fig. S.1). Both crystals seemed to appear simultaneously and in the same proportions throughout the reaction. The amount of parallelepipedic crystal decreased with increasing temperature but increased with increasing concentration (Fig. S.2).

Fig. 2 shows representative images of hexagonal platelets obtained at different concentrations and temperatures. In general, the diameter increased with the reagent concentration, but was not markedly affected by a change of temperature. A change of concentration also affected the aspect ratio and the shape of the particles: hexagonal prisms with well-defined edges and low aspect ratios (~ 3) were noticed at low concentration, whereas thinner discs with higher aspect ratios (>10) were observed at high concentration. Variations in surface appearance were noticed, like the presence of porosities in some samples. This was also already observed by Galea et al. [21] and attributed to the rinsing process.

4.3. XRD results

Rietveld refinement of XRD measurements performed on samples retrieved at the end of the synthesis reaction revealed the presence of three calcium phosphate phases: β -TCP, DCP (CaHPO_4) and chloro-apatite ($\text{Ca}_5(\text{PO}_4)_3(\text{OH},\text{Cl})$) (Fig. 3). The monetite fraction was the highest at low temperature and high concentration (Table 1). For example, 79 wt.% DCP was measured at 90 °C and 16 mM. The DCP fraction decreased then with increasing temperature and decreasing concentration. Since the Cl-Ap content remained very low (<10%) in all samples, a decrease in DCP content resulted in an increase in β -TCP content. As a result, pure β -TCP samples were obtained in various conditions, for example at a concentration of 4 mM at 130 °C and 150 °C, and at a concentration of 16 mM at 150 °C. Looking at the SEM images, the hexagonal prisms were identified as the β -TCP phase, the parallelepiped crystals as DCP and rare small elongated particles as Cl-Ap.

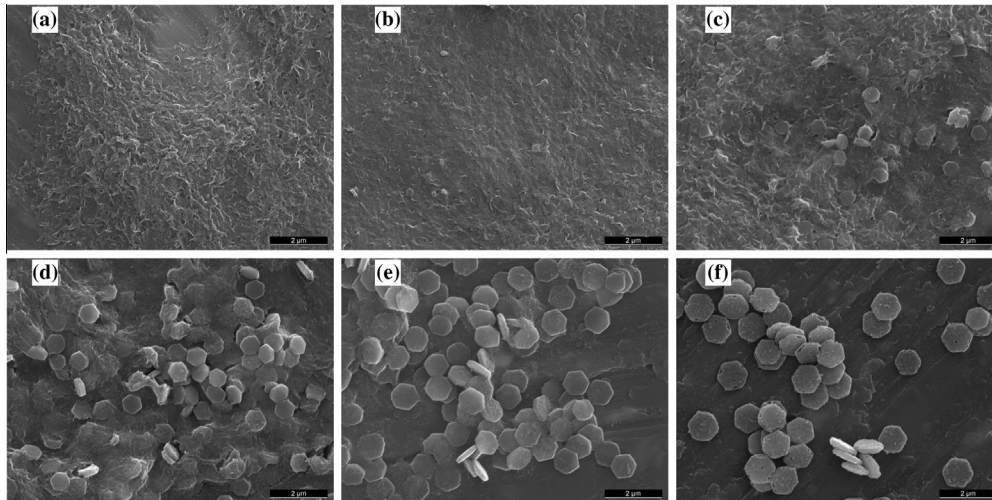


Fig. 1. SEM images of samples taken out of the reactor at 150 °C at different times: (a) 10 s; (b) 30 s; (c) 70 s; (d) 90 s; (e) 2 min; (f) 24 h. The scale bars are 2 μ m.

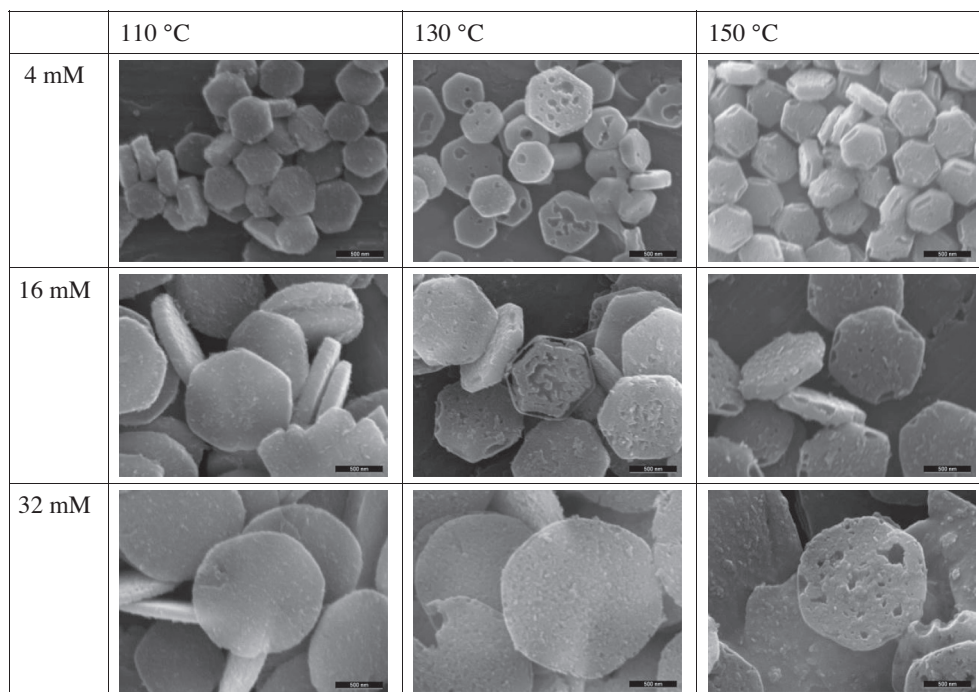


Fig. 2. SEM images of samples after complete reaction at different temperatures (110, 130, 150 °C) and concentrations (4, 16, 32 mM). The scale bar is 500 nm for all images.

4.4. Size measurements

At all reaction temperatures, the hexagonal crystals grew continuously in diameter and thickness until a plateau was reached (Fig. 4a and b). Higher reaction temperatures strongly accelerated the nucleation and growth of the crystals, while a concentration increase had a much smaller effect (this can also be appreciated in linear scale, Fig. S.3). However, concentration markedly affected the plateau diameter value (Fig. 4a and b). The aspect ratio tended to slightly increase during the fast crystal growth at the beginning of the reaction, but hardly varied at long reaction times (Fig. 4c). The size dispersion was quite constant with reaction time, and was the highest at low temperature or low concentration (Fig. 4d). The final size and aspect ratio increased with the concentration, and slightly varied with temperature changes (Fig. 4e–g). The largest variations were observed between 150 and 170 °C,

where the diameter and aspect ratio clearly decreased. The hexagonal platelets first decreased in diameter, without large changes of thickness (Fig. 5a) and then became round at 170 °C (Fig. 5b). The size dispersion at the end of the precipitation reaction was generally between 0.05 and 0.10. However, there were some exceptions (Figs. 4h and 5a).

4.5. Kinetic calculations

β -TCP growth was the fastest at the beginning of the reaction, when the particles were still small and the amount of precursors was high. As the precipitation continued, the precursor concentration decreased, the particle size increased and the growth rate decreased (Fig. 6a).

The observed growth curves were fitted numerically with a reaction-controlled and a diffusion-controlled model (Eqs. (6)

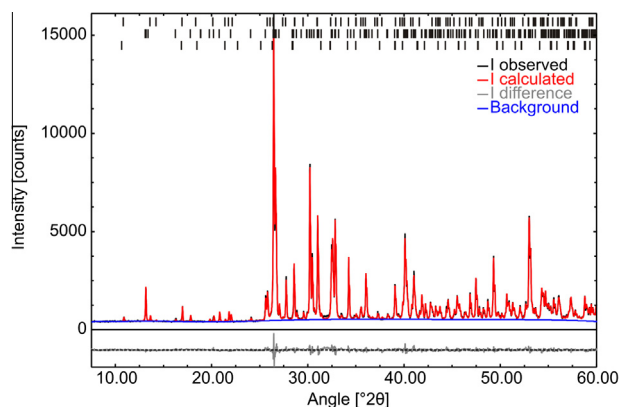


Fig. 3. Representative XRD diffractogram of particles synthesized at 90 °C, 16 mM for 24 h showing the presence of highly crystalline β -TCP and DCP phases. Observed, calculated, differences and background intensities are displayed, as well as the hkl line positions for β -TCP (top), DCP (middle) and Cl-Ap (bottom).

and (7); Fig. 6a). Importantly, the values of $[M_0]$ were corrected with the phase analysis from the XRD results (Table 1) to only consider the amounts of precursors that were effectively used to grow the β -TCP particles and neglect the ions that were used to grow other crystalline phases (comparisons with uncorrected $[M_0]$ values are presented in Supplementary data, Fig. S.4). Both equations led to good fits, with average regression coefficients (R^2) > 0.94 in both cases. Two of the 14 experiments could not be fitted properly due to a lack of experimental data point in the growing phase. Seven experiments were slightly better fitted with the diffusion-controlled equation and five were slightly better fitted with the surface-controlled equation, but the differences in R^2 values never exceeded 0.03. Fitting the data with the surface-controlled model led to nucleation times close to zero, while using the diffusion-controlled model led to positive nucleation times, increasing up to a few minutes at low reaction temperatures (Supplementary data, Fig. S.5). Interestingly, the diffusion coefficients calculated with Eq. (7) were extremely low, typically close to 10^{-14} m² s. Such low diffusion coefficients suppose very large diffusion entities (see Supplementary data, Fig. S.6). The growth rate strongly increased with an increase of temperature but was only slightly affected by the precursor concentration (Fig. 6b). The activation energy for the crystallization reaction was obtained by plotting the reaction constant as a function of the inverse of temperature (Fig. 6b). Values of 88 ± 16 , 78 ± 3 and 102 ± 19 kJ mol⁻¹ were obtained at 4, 16 and 32 mM.

The particle concentration was also retrieved from the numerical fits (Eq. (9), Fig. 6c). With the exception of the particles obtained at 170 °C, the particle concentration did not vary much

with temperature and appeared to be independent of the initial concentration.

5. Discussion

The aim of the present study was to determine the growth kinetics of β -TCP particles, with the aim that a better control of the aspect ratio of β -TCP particles could eventually be achieved. For that purpose, β -TCP particles were produced at various concentrations (4, 16 and 32 mM) and temperatures (from 90 to 170 °C) since Levenspiel [27] mentioned that these were the two most important parameters affecting the growth kinetics of particles.

5.1. Nucleation and assembly mechanism

In the current study, a gel-like substance was detected in the first stages of the reaction and could be separated from the supernatant by centrifugation. This observation suggests that this gel consisted of a large continuous structure, because if it were made of small individual parts, they would not sediment by centrifugation. Tao et al. [20,28] identified this phase as amorphous and suggested that β -TCP crystals form according to the crystallization process proposed by Gebauer and Cölfen [29]: β -TCP crystals nucleate within an amorphous phase and grow by solid conversion. However, as underlined by Hu et al. [30], it is very difficult to differentiate between the latter mechanism and a simple dissolution–precipitation reaction. Since no transmission electron microscopy observations were performed in the present study to follow the occurrence and growth of β -TCP nuclei, it is not possible to contradict or confirm the theory of Tao et al. Other nucleation mechanisms could be used to describe the nucleation of β -calcium phosphate [31–34] but such a discussion is beyond the scope of this work.

Nevertheless, several important observations can be made. First, the various numerical fits performed in the frame of this study (Fig. 6a) suggest that β -TCP particles formed very early in the synthesis reaction or, in other words, that the nucleation time was very short or even instantaneous. Indeed, even though the nucleation time was a fitting parameter, its value was mostly equal to zero in the surface-controlled model. Second, small β -TCP crystals were only observed at the initial stages of the reaction (Figs. 1 and S.1). Third, the particle size distribution remained very narrow throughout the reaction (Fig. 4d). Kwon and Hyeon [22] referred to this phenomenon as a “burst nucleation”. In such a case, the concentration rapidly drops after particle nucleation, hence impairing further nucleation and promoting crystal growth [22]. As a consequence, all crystals reach roughly the same size at the same moment (for a given temperature) and the crystal size distribution is very narrow all along crystal growth (Fig. 4d). This emphasizes

Table 1
Crystalline composition (wt.%) as a function of temperature and concentration (Rietveld refinement of XRD diffractograms). The values are averages \pm standard deviations except when only one XRD measurement could be performed.

Concentration of precursors	Crystalline phase	Temperature				
		90 °C	110 °C	130 °C	150 °C	170 °C
4 mM	β -TCP	na	97 \pm 4%	100%	100 \pm 0%	na
	DCP	na	3 \pm 4%	0%	0 \pm 0%	na
	Cl-Ap	na	0 \pm 0%	0%	0 \pm 0%	na
16 mM	β -TCP	17 \pm 2%	66 \pm 5%	93 \pm 3%	100 \pm 1%	99 \pm 2%
	DCP	79 \pm 6%	34 \pm 5%	3 \pm 0%	0 \pm 0%	0 \pm 0%
	Cl-Ap	3 \pm 5%	3 \pm 0%	2 \pm 3%	0 \pm 0%	1 \pm 2%
32 mM	β -TCP	na	55%	72%	90 \pm 3%	na
	DCP	na	45%	28%	1 \pm 1%	na
	Cl-Ap	na	0%	0%	9 \pm 4%	na

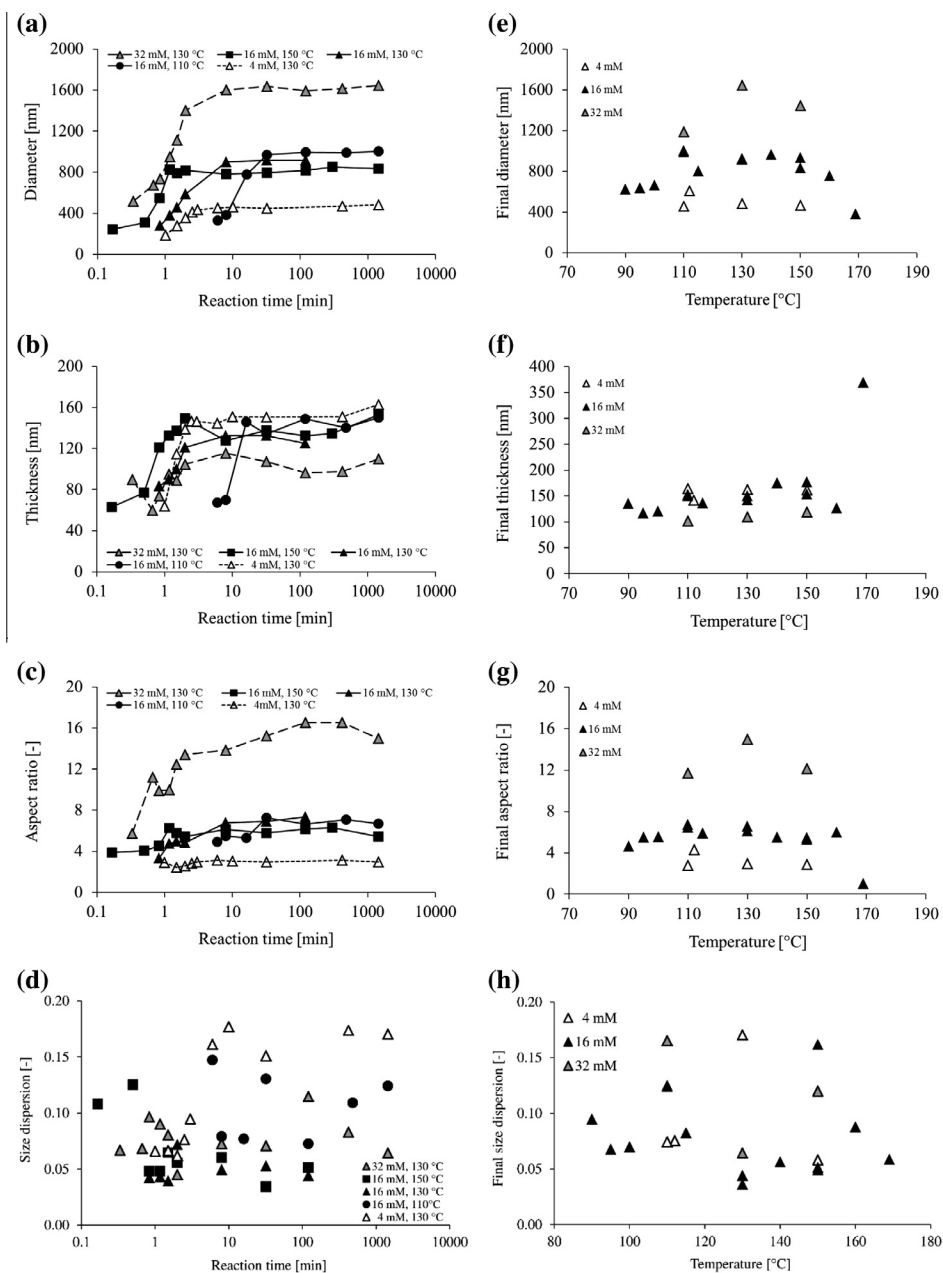
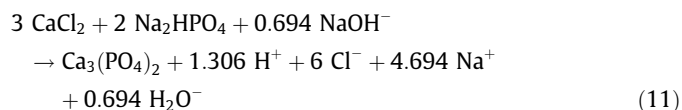


Fig. 4. Evolution of the platelet (a) diameter, (b) thickness, (c) aspect ratio and (d) size dispersion as a function of the reaction time at different temperatures ((●) 110 °C, (▲, △, ▲) 130 °C, (■): 150 °C) and concentrations (results only at 130 °C: (△) 4 mM, (▲) 16 mM, (▲) 32 mM). Final platelet (e) diameter, (f) thickness, (g) aspect ratio and (h) size dispersion at different temperatures and concentrations.

that the nucleation process in the present system can effectively be neglected in the kinetics study of the growing phase. Even though the data collected in this study follow Kwon's theory, a more detailed look shows that nucleation cannot stop due to a drop of concentration. Indeed, nucleation was very rapid in samples containing a 4 mM precursor concentration. So, logically, nucleation should be very intense during the consumption of at least 12 mM of the precursors in samples containing a 16 mM initial precursor concentration. Also, an increase of precursor concentration should increase the number of particles and decrease their size. However, this was not observed experimentally, suggesting that a different mechanism must occur.

So far, it was assumed that pH (or rather H/OH ratios) values were kept constant. Indeed, the $\text{Na}_2\text{HPO}_4/\text{NaOH}$ molar ratio (=2.88) was kept constant throughout the experiments. However,

since Tao et al. [28] mentioned that the gel had a chemical composition close to that of β -TCP, its formation should acidify the solution via the following reaction:



Preliminary in situ pH measurements support this explanation. From Eq. (11), the absolute amount of H^+ ions released during the reaction is expected to increase with the precursor concentration, i.e. lower pH values would be present within the precipitation reaction at high precursor concentrations. Since calcium phosphate solubility increases with a decrease of pH [35], the increase of supersaturation due to the increase in the initial precursor

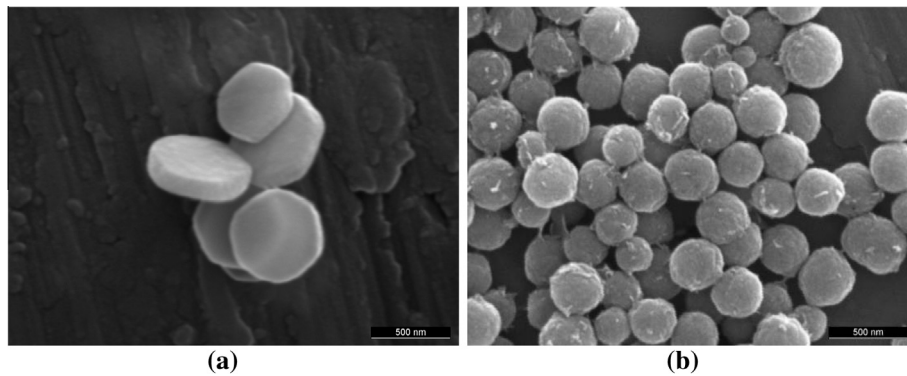


Fig. 5. SEM of samples after complete reaction at 16 mM and (a) 160 °C; (b) 170 °C. Above 150 °C, the particle size and aspect ratio clearly decrease. The particles in (a) are discs, whereas in (b) they are spherical. Scale bars are 500 nm in (a) and (b).

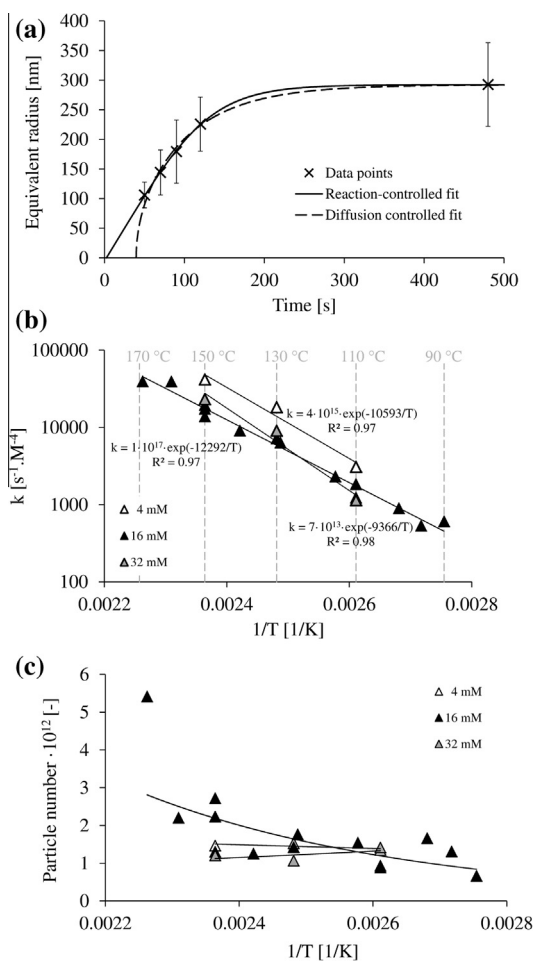


Fig. 6. (a) Example of a fit of $r(t)$ at 130 °C, 16 mM; (b) reaction rate coefficient as a function of $1/T$ for (Δ) 4 mM, (\blacktriangle) 16 mM, (\triangle) 32 mM of precursors; (c) Number of particles as a function of $1/T$ for 4, 16 and 32 mM of precursors.

concentration could be annealed by the decrease of pH. This could explain why a change of concentration from 4 to 32 mM did not lead to an eight-fold increase in particle concentration.

Once the crystallization reaction was completed, β -TCP crystals did not change in size or shape. For example, no change of crystal size and shape was observed between 2 min and 24 h of reaction at 16 mM and 150 °C (Fig. 1). This is surprising because Ostwald [36] predicted that small crystals should dissolve and redeposit on the surfaces of large thermodynamically more stable crystals [37].

However, Ostwald ripening occurs when the driving force for crystallization is weak, i.e. some particles may dissolve, while others keep growing. In fact, it depends on the sensitivity of the solubility to the size of the particles. If it is high, as for nanocrystals, then the smallest easily dissolve and the largest grow more, but for larger particles the effect of Ostwald ripening is much lower [38]. In the present case, the particles were apparently large enough to keep this phenomenon low in most cases. Indeed, the size distribution tended to become broader at lower temperatures and concentrations (Fig. 4d), i.e. at lower supersaturation [39]. In practice, this result suggests that longer reaction times cannot be used to enhance the platelet diameter and aspect ratio.

5.2. Reaction kinetics

Large amounts of monetite were detected at low temperature and high concentration. However, there was no evidence that the formation of this calcium phosphate phase affected β -TCP precipitation and thus its kinetics. Indeed, the reaction constants obtained at low temperature did not deviate much from the regression line $k = f(1/T)$ (Fig. 6b). Strong effects would be expected if DCP formed before β -TCP, but since it was not possible to perform XRD measurements during the synthesis reaction (too small aliquots), the sequence of calcium phosphate formation could not be determined. Also, SEM measurements did not reveal a clear difference in the time of DCP and β -TCP formation.

The experimental data collected in this study suggests that under the used conditions β -TCP growth is not diffusion-controlled, but reaction-controlled, even if both models show good fits (Fig. 6a). First, no change of reaction rate was observed with a change of concentration (Fig. 6b), which is unexpected for a diffusion-controlled reaction. Second, the diffusion coefficients calculated with the diffusion-controlled model were clearly unrealistic. Third, the high activation energies are characteristic of surface-controlled reactions, and last, Kwon and Hyeon [22] mentioned that the growth of sub-micrometric particles is generally reaction-controlled.

In the kinetics analysis performed here, it was assumed that the retrieval time corresponded to the reaction time. However, it took a few seconds to aspirate the sample and to cool it down. Therefore, it is likely that the reaction time was slightly underestimated. Whereas it did not really matter for long reaction times or slow reactions at low temperature, it certainly mattered for aliquots retrieved within the first minute of reaction for reactions performed at high temperature. These very fast reactions also limited the number of samples that could be retrieved during crystal growth. At lower temperatures, other problems were encountered. Indeed, it was difficult to precisely control the temperature during the

whole crystallization because the reactions extended over several hours.

5.3. Control of size and aspect ratio

Temperature changes hardly influenced β -TCP crystal size and shape except for a strong decrease at very high temperature, Figs. 4e–g and 5. However, it is a useful mean to limit monetite formation (Table 1), accelerate β -TCP synthesis (Fig. 6b) and narrow β -TCP size dispersion (Fig. 4h).

The results presented in this study show that β -TCP platelets grew mostly in width and not in thickness (Fig. 4). Moreover, the nucleation was apparently insensitive to concentration changes (Fig. 6c). Therefore, a change of the precursor concentration is expected to strongly affect the β -TCP aspect ratio. Indeed, increasing the concentration appeared to be the most efficient way to increase the diameter and aspect ratio of β -TCP platelets (Figs. 2 and 4). Unfortunately, the solubility of the phosphate precursor was limited and DCP and Cl-Ap precipitated at high precursor concentrations (Table 1). The presence of DCP at high concentration was explained by Galea et al. [21] by an acidification of the solution due to H^+ release from the Na_2HPO_4 precursor (See Eq. (11)). Indeed, DCP is stabilized at low pH [35]. Hence, more NaOH might be necessary to maintain the H^+ amount independently of the concentration. A few preliminary tests were done, but increasing the OH^- amount clearly slowed down β -TCP growth and strongly delayed nucleation, leading to mainly amorphous samples. Also, the aspect ratio was reduced. A continuous titration over time might be a better solution, but is difficult to apply here due to the difficulties in measuring a pH value in a non-aqueous medium above 100 °C.

Since the thickness of β -TCP particles was hardly affected by changes of the crystallization conditions, another approach to control the particle size would be to decrease the number of particles. For example, an increase in the surface energy of the nuclei should increase the critical size, hence decreasing the nucleation rate and the number of nuclei [22]. This approach will be considered in future experiments, with for example a solvent change, addition of foreign ions or change of precursors, as Tao et al. demonstrated that this might influence the crystal face stability.

As a last note, the formation of almost spherical β -TCP particles at 170 °C (Fig. 5b) has to be underlined. To the best of our knowledge, this is the first study reporting the synthesis of such shaped particles with an average particle size of ≈ 400 nm. In our previous paper [21], the particles obtained at 170 °C more closely resembled those presently obtained at 160 °C (Fig. 5a). This difference might be explained by an improvement in the control of the temperature during the initial stages of the reaction.

6. Conclusions

The precipitation of calcium and phosphate ions in ethylene glycol effectively led to the production of sub-micrometric β -TCP hexagonal platelets. The reaction temperature had a strong influence on the reaction rate but hardly affected the β -TCP platelets size (diameter ≈ 600 –1000 nm) and aspect ratio ($s \approx 4.5$ –6.5). The precursor concentration strongly influenced the size and aspect ratio of the platelets (diameter ≈ 400 –1700 nm and $s \approx 3$ –15), but with no significant influence on the reaction kinetics. The analysis of the numerical fits of the growth curves revealed that the reaction was most likely reaction-controlled even though excellent fits were also obtained with a diffusion-controlled model ($R^2 > 0.94$). This conclusion was supported by the high activation energies (close to 80–100 kJ mol $^{-1}$) and the very low diffusion coefficients calculated from the fits. A surprising result was the fairly constant number of particle observed in the different exper-

iments conducted at various concentrations. As a result, the particle diameter strongly increased with an increase in the precursor concentration (five-fold increase for an eight-fold increase in concentration).

Working at high concentrations and high temperature is advantageous to rapidly produce platelets with large diameter and aspect ratio of the platelets, but high concentrations also lead to an increase of monetite and Cl-Ap by-product, i.e. inhomogeneities in composition and size. Hence the maximum aspect ratio seen for pure β -TCP samples was limited to 5–6. Ideal working conditions for phase-pure β -TCP of high aspect ratio were found at 16 mM concentration, 150 °C and >2 min reaction time.

Appendix A. Figures with essential colour discrimination

Certain figure in this article, particularly Fig. 3, is difficult to interpret in black and white. The full colour images can be found in the on-line version, at <http://dx.doi.org/10.1016/j.actbio.2014.02.044>.

Appendix B. Supplementary data

Supplementary data associated with this article can be found, in the online version, at <http://dx.doi.org/10.1016/j.actbio.2014.02.044>.

References

- [1] Banwart JC, Asher MA, Hassanein RS. Iliac crest bone graft harvest donor site morbidity. A statistical evaluation. *Spine* 1995;20(9):1055–60.
- [2] Younger EM, Chapman MW. Morbidity at bone graft donor sites. *J Orthop Trauma* 1989;3(3):192–5.
- [3] Hofmann GO, Kirschner MH, Wangemann T, Falk C, Mempel W, Hammer C. Infections and immunological hazards of allogeneic bone transplantation. *Arch Orthop Trauma Surg* 1995;114(3):159–66.
- [4] Giannoudis PV, Dinopoulos H, Tsiroidis E. Bone substitutes: an update. *Injury* 2005;36(Suppl. 3):S20–27.
- [5] LeGeros RZ. Properties of osteoconductive biomaterials: calcium phosphates. *Clin Orthop* 2002;395:81–98.
- [6] Bohner M. Resorbable biomaterials as bone graft substitutes. *Mater Today* 2010;13(1–2):24–30.
- [7] Eggli PS, Muller W, Schenk RK. Porous hydroxyapatite and tricalcium phosphate cylinders with two different pore size ranges implanted in the cancellous bone of rabbits. A comparative histomorphometric and histologic study of bony ingrowth and implant substitution. *Clin Orthop* 1988;232:127–38.
- [8] Wagoner Johnson AJ, Herschler BA. A review of the mechanical behavior of CaP and CaP/polymer composites for applications in bone replacement and repair. *Acta Biomater* 2011;7(1):16–30.
- [9] Rezwan K, Chen QZ, Blaker JJ, Boccaccini AR. Biodegradable and bioactive porous polymer/inorganic composite scaffolds for bone tissue engineering. *Biomaterials* 2006;27(18):3413–31.
- [10] Tang Z, Kotov NA, Magonov S, Ozturk B. Nanostructured artificial nacre. *Nat Mater* 2003;2(6):413–8.
- [11] Dimas LS, Bratzel GH, Eylon I, Buehler MJ. Tough composites inspired by mineralized natural materials: computation, 3D printing, and testing. *Adv Funct Mater* 2013;23(36):4629–38.
- [12] Bonderer LJ, Studart AR, Gauckler LJ. Bioinspired design and assembly of platelet reinforced polymer films. *Science* 2008;319(5866):1069–73.
- [13] Ji B, Gao H. Mechanical properties of nanostructure of biological materials. *J Mech Phys Solids* 2004;52:1963–90.
- [14] Barthelat F. Biomimetics for next generation materials. *Philos Trans R Soc A Math Phys Eng Sci* 1861;2007(365):2907–19.
- [15] Kamat S, Su X, Ballarini R, Heuer AH. Structural basis for the fracture toughness of the shell of the conch *Strombus gigas*. *Nature* 2000;405(6790):1036–40.
- [16] Meyers MA, Chen PY, Lin AYM, Seki Y. Biological materials: structure and mechanical properties. *Prog Mater Sci* 2008;53(1):1–206.
- [17] Griffith AA. The phenomena of rupture and flow in solids. *Philos Trans R Soc Lond A (Containing Papers of a Mathematical or Physical Character)* 1921;221:163–98.
- [18] Gao H. Application of fracture mechanics concepts to hierarchical biomechanics of bone and bone-like materials. *Int J Fract* 2006;138(1–4):101–37.
- [19] Jackson AP, Vincent JFV, Turner RM. The mechanical design of nacre. *Proc R Soc Lond B Biol Sci* 1988;234(1277):415–40.
- [20] Tao J, Jiang W, Zhai H, Pan H, Xu R, Tang R. Structural components and anisotropic dissolution behaviors in one hexagonal single crystal of β -tricalcium phosphate. *Cryst Growth Des* 2008;8(7):2227–34.

- [21] Galea L, Bohner M, Thuering J, Doebelin N, Aneziris CG, Graule T. Control of the size, shape and composition of highly uniform, non-agglomerated, sub-micrometer β -tricalcium phosphate and dicalcium phosphate platelets. *Biomaterials* 2013;34:6388–401.
- [22] Kwon SG, Hyeon T. Formation mechanisms of uniform nanocrystals via hot-injection and heat-up methods. *Small* 2011;7(19):2685–702.
- [23] Rodriguez-Carvajal J. Recent developments of the program FULLPROF. Commission on powder diffraction (IUCr). *Newsletter* 2001;26:12–9.
- [24] Schroeder LW, Dickens B, Brown WE. Crystallographic studies of the role of Mg as a stabilizing impurity in β - $\text{Ca}_3(\text{PO}_4)_2$. II. Refinement of Mg-containing β - $\text{Ca}_3(\text{PO}_4)_2$. *J Solid State Chem* 1977;22(3):253–62.
- [25] Dickens B, Bowen JS, Brown WE. A refinement of the crystal structure of CaHPO_4 (synthetic monetite). *Acta Crystallogr* 1971;B28:797–806.
- [26] Hughes JM, Cameron M, Crowley KD. Structural variations in natural F, OH, and Cl apatites. *Am Mineral* 1989;74(7–8):870–6.
- [27] Levenspiel O. *Chemical reaction engineering*. 2nd ed. New York: John Wiley; 1972.
- [28] Tao J, Pan H, Zhai H, Wang J, Li L, Wu J, et al. Controls of tricalcium phosphate single-crystal formation from its amorphous precursor by interfacial energy. *Cryst Growth Des* 2009;9(7):3154–60.
- [29] Gebauer D, Cölfen H. Prenucleation clusters and non-classical nucleation. *Nano Today* 2011;6(6):564–84.
- [30] Hu Q, Nielsen MH, Freeman CL, Hamm LM, Tao J, Lee JRI, et al. The thermodynamics of calcite nucleation at organic interfaces: classical vs. non-classical pathways. *Faraday Discuss* 2012;159:509–23.
- [31] Baumgartner J, Dey A, Bomans PHH, Le Coadou C, Fratzl P, Sommerdijk NAJM, et al. Nucleation and growth of magnetite from solution. *Nat Mater* 2013;12(4):310–4.
- [32] Dorvee JR, Veis A. Water in the formation of biogenic minerals: peeling away the hydration layers. *J Struct Biol* 2013;183(2):278–303.
- [33] Wolf SE, Leiterer J, Kappl M, Emmerling F, Tremel W. Early homogenous amorphous precursor stages of calcium carbonate and subsequent crystal growth in levitated droplets. *J Am Chem Soc* 2008;130(37):12342–7.
- [34] Habraken WJEM, Tao J, Brylka LJ, Friedrich H, Bertinetti L, Schenk AS, et al. Ion-association complexes unite classical and non-classical theories for the biomimetic nucleation of calcium phosphate. *Nat Commun* 2013;4. Article number 1507.
- [35] Vereecke G, Lemaitre J. Calculation of the solubility diagrams in the system $\text{Ca}(\text{OH})_2$ - H_3PO_4 - KOH - HNO_3 - CO_2 - H_2O . *J Cryst Growth* 1990;104:820–32.
- [36] Ostwald W. Studien über die Bildung und Umwandlung fester Körper. *Z Phys Chem* 1897;22:289.
- [37] Wilkinson ADMAA. IUPAC. *Compendium of chemical terminology (the "Gold Book")*. Oxford: Blackwell Scientific Publications; 1997.
- [38] Talapin DV, Rogach AL, Haase M, Weller H. Evolution of an ensemble of nanoparticles in a colloidal solution: theoretical study. *J Phys Chem B* 2001;105(49):12278–85.
- [39] Sugimoto T. Preparation of monodispersed colloidal particles. *Adv Colloid Interface Sci* 1987;28(C):65–108.